

- [15] In order to form thin films for vitrification, it was necessary to load the grids with warm gelator solution that had not yet gelled. The solution was then allowed to cool slightly, beginning the gelation process, on the grid before blotting and plunging (see Experimental). In this way we were able to capture the initial aggregation before complete gelation made it impossible to form thin films. The use of glow-charged grids was found to facilitate the formation of uniformly thin, well-formed films.
- [16] R. Oda, I. Huc, M. Schmutz, S. J. Candau, F. C. MacKintosh, *Nature* **1999**, 399, 566.
- [17] SEM images of the dried and rinsed gel of **1** indicated a fibrous structure [2].
- [18] a) J. H. Fuhrhop, W. Helfrich, *Chem. Rev.* **1993**, 93, 1565. b) E. R. Zubarev, M. U. Pralle, E. D. Sone, S. I. Stupp, *Adv. Mater.* **2002**, 14, 198. c) J. V. Selinger, M. S. Spector, J. M. Schnur, *J. Phys. Chem. B* **2001**, 105, 7157. d) I. Nakazawa, M. Masuda, Y. Okada, T. Hanada, K. Yase, M. Asai, T. Shimizu, *Langmuir* **1999**, 15, 4757.
- [19] J. H. Jung, H. Kobayashi, M. Masuda, T. Shimizu, S. Shinkai, *J. Am. Chem. Soc.* **2001**, 123, 8785.
- [20] As previously reported, at pH 5.9, **2** forms a gel, suggesting that its molecular aggregation is related to **1** [2].
- [21] As part of the powder indexing module of Cerius<sup>2</sup>: P. E. Werner, L. Eriksson, M. Westdahl, *J. Appl. Crystallogr.* **1985**, 18, 367.
- [22] a) K. D. M. Harris, M. Tremayne, B. M. Kariuki, *Angew. Chem. Int. Ed.* **2001**, 40, 1626. b) P. J. Prest, R. B. Prince, J. S. Moore, *J. Am. Chem. Soc.* **1999**, 121, 5933. c) C. W. Struijk, A. B. Sieval, J. E. J. Dakhorst, M. van Dijk, P. Kimkes, R. B. M. Koehorst, H. Donker, T. J. Schaafsma, S. J. Picken, A. M. van de Craats, J. M. Warman, H. Zuilhof, E. J. R. Sudholter, *J. Am. Chem. Soc.* **2000**, 122, 11057. d) S. Ito, M. Wehmeier, J. D. Brand, C. Kubel, R. Epsch, J. P. Rabe, K. Mullen, *Chem. Eur. J.* **2000**, 6, 4327. e) M. E. Amato, R. Caminiti, G. A. Carriedo, E. J. Garcia-Alonso, J. L. Garcia-Alvarez, G. M. Lombardo, G. C. Pappalardo, *Chem. Eur. J.* **2001**, 7, 1486.
- [23] L. Leiserowitz, A. T. Hagler, *Proc. R. Soc. London, Ser. A* **1983**, 388, 133.
- [24] J. Bernstein, M. C. Etter, L. Leiserowitz, in *Structure Correlation, Vol. 2* (Eds: H.-B. Burgi, J. D. Dunitz), John Wiley & Sons, New York **1994**, p. 431.
- [25] Experimentally, using the flotation technique in a carbon tetrachloride/heptane mixture, the density of the fibers is between 1.6 and 1.3 g cm<sup>-3</sup>.
- [26] G. H. Stout, L. H. Jensen, *X-ray Structure Determination – A Practical Guide*, 2nd ed., John Wiley & Sons, New York **1989**.
- [27] S. B. Kennedy, E. R. deAzevedo, W. A. Petka, T. P. Russell, D. A. Tirrell, M. Hong, *Macromolecules* **2001**, 34, 8675.
- [28] J. Dubochet, M. Groom, S. Mueller-Neuteboom, in *Advances in Optical and Electron Microscopy, Vol. 8* (Eds: R. Barer, V. E. Cosslett), Academic Press, New York **1982**, p. 107.

## Isolated Single-Molecule Magnets on the Surface of a Polymeric Thin Film\*\*

By Daniel Ruiz-Molina, Marta Mas-Torrent, Jordi Gómez, Ana I. Balana, Neus Domingo, Javier Tejada, María T. Martínez, Concepció Rovira, and Jaume Veciana\*

Single-molecule magnets (SMMs) have a large-spin ground state with appreciable magnetic anisotropy, resulting in a barrier for spin reversal.<sup>[1]</sup> As a consequence, interesting mag-

netic properties such as out-of-phase ac magnetic susceptibility signals and stepwise magnetization hysteresis loops are observed. In addition to resonant magnetization tunneling<sup>[2-4]</sup> several other interesting phenomena have also been reported during the past few years.<sup>[5-9]</sup> The origin of slow magnetization relaxation rates as well as of other phenomena is due to individual molecules rather than to long-range ordering, as confirmed by magnetization relaxation and heat-capacity studies.<sup>[10]</sup> Therefore, SMMs represent nanoscale magnetic particles of a sharply defined size that offer potential access to ultimate high-density information storage devices<sup>[11]</sup> and quantum-computing applications.<sup>[12,13]</sup> However, if a truly molecular computational device based on an SMM is to be achieved, new systematic studies are required that encompass ways of addressing properly oriented individual molecules or molecular aggregates onto the surface of a thin film, where each molecule or molecular aggregate can be used as a bit of information. The first approach to arrange SMMs into well-organized multilayered films was undertaken by means of the Langmuir–Blodgett (LB) technique.<sup>[14]</sup> Although these self-assembled monolayer films are transferable to other substrates, there are limitations to their practical utilization since these LB films may become unstable especially due to incompatible surface energies.

Here we report a new soft, reliable, and simple methodology to address individual Mn<sub>12</sub> complexes onto a film surface. Such a methodology is based on the preparation of polymeric thin films, made from a polycarbonate matrix and a Mn<sub>12</sub> complex, and subsequent treatment with different organic solvent vapors. Solvent treatment leads to the emerging of a small fraction of the Mn<sub>12</sub> molecules to the surface of the film with an aggregation state that can be controlled at will, depending on the nature of the solvent. It has already been established that after absorption of suitable amounts of a solvent that is capable of effectively solvating the polymer chains, the swollen polymer network exhibits an enhanced porosity.<sup>[15]</sup> This situation provides a valuable route for the molecular reorganization of the nanocomposite with a small fraction of Mn<sub>12</sub> molecules (approximately 0.1 %) emerging to the film surface.

Imaging of the thin film prior to and after solvent treatment using scanning electron microscopy (SEM) does not provide any information on solvent effects except for a solvent-induced surface-smoothing process. Resolution of any structure at the nanometer scale without beam-induced damage proved difficult, therefore atomic force microscopy (AFM) studies were performed. Firstly, high-resolution AFM images of a thin film that was treated with the vapor of a 1:1 CH<sub>2</sub>Cl<sub>2</sub>/hexane mixture were obtained. The top-view topographical images and the corresponding height profiles across surface locations, which are indicated in the topographical images, are shown in Figure 1. In the same figure, the corresponding 3D-AFM topography images are also shown (Fig. 1b and 1e). The images show many semi-globular islands located on the film surface, a pattern that was confirmed after additional measurements made in a minimum of three different well-

[\*] Prof. J. Veciana, Dr. D. Ruiz-Molina, Dr. M. Mas-Torrent, J. Gómez, Dr. C. Rovira  
Institut de Ciència de Materials de Barcelona (CSIC)  
Campus Universitari de Bellaterra, E-08193 Cerdanyola (Spain)  
A. I. Balana, Dr. M. T. Martínez  
Instituto de Carboquímica (CSIC)  
Miguel Luesma Castan 4, E-50015 Zaragoza (Spain)  
N. Domingo, Prof. J. Tejada  
Facultad de Física, Universitat de Barcelona  
Diagonal 647, E-08028 Barcelona (Spain)

[\*\*] This work was supported by the Information Society Technologies Programme of the European Commission, as part of the project NANOMAGIQC, and the Programa Nacional de Materiales de la Dirección General de Investigación (Spain), as part of the project MAGMOL.

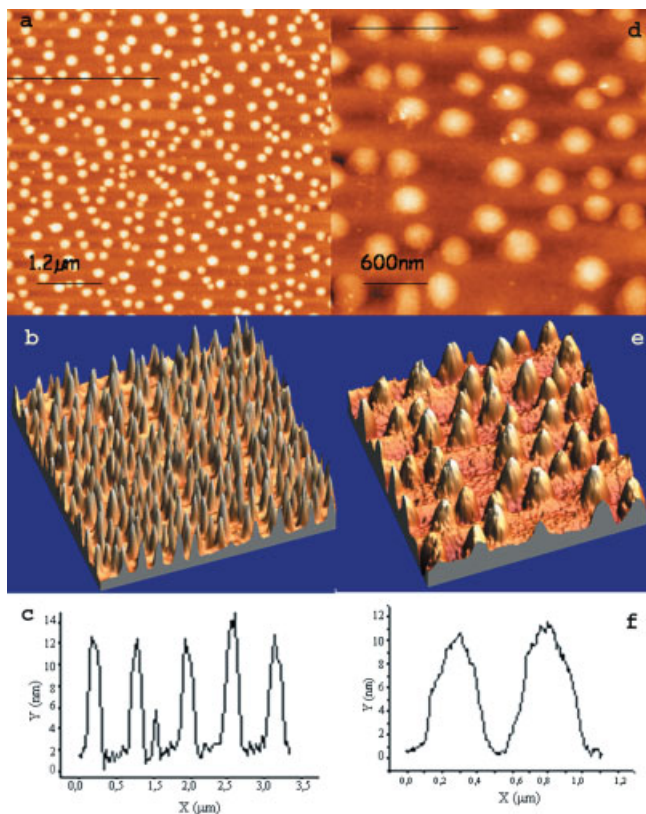


Fig. 1. AFM images of nanocomposite films, made from a polycarbonate polymeric matrix and the  $Mn_{12}$  complex, which have been treated with  $CH_2Cl_2$ /hexane (1:1). The left part of the figure shows islands on a  $10 \times 10 \mu m$  surface. a) Topographical top-view. b) 3D image of the same area. c) Height profile. The right part of the figure (d–f) shows data for a  $3 \times 3 \mu m$  surface. The height profiles in (c) and (f) are taken at the location indicated by the black lines in (a) and (d), respectively.

separated  $10 \times 10 \mu m$  sites. In each of the images, the particles appear to be relatively uniform in size, with an experimental averaged height of  $12 \pm 1$  nm.

A detailed study of the molecular structure of the  $Mn_{12}$  complex used in this paper showed that this complex exhibits an averaged structure with a coin-like shape with two different end-to-end distances.<sup>[16]</sup> This result was obtained by the minimization of its structure with a force-field method. The largest end-to-end distance was found to be almost 4 nm, whereas the shortest was 3 nm. Therefore, as each of the islands observed using AFM has an average height of 12 nm, it must contain at least three or four  $Mn_{12}$  molecules. On the other hand, the averaged observed full width at the baseline level, which is approximately 250 nm, is evidently larger than the expected width for four aggregated  $Mn_{12}$  molecules. The origin for such deviation may be attributed either to the presence of more than four  $Mn_{12}$  molecules at the basal plane and/or to geometrical AFM-tip convolution effects.<sup>[17]</sup> Finally, it has to be mentioned that AFM images of thin films preceding solvent treatment exhibit rather uneven and rough surfaces with the lack of any semi-globular islands.

The formation of molecular aggregates of the  $Mn_{12}$  complex in the form of islands is explained well by the large num-

ber of phenyl rings present in this complex, which may cause them to aggregate mainly due to attractive  $\pi$ - $\pi$  interactions. The solvent mixture used favors such aggregation. Indeed, the  $Mn_{12}$  complex is highly soluble in  $CH_2Cl_2$  but not in hexane. This situation certainly favors the formation of aggregates. For this reason, a new polymeric thin film was exclusively exposed to  $CH_2Cl_2$  vapor to address individual molecules rather than aggregates of several molecules onto the film surface. The topographical top-view and the corresponding 3D images along with some profiles across surface locations are shown in Figure 2. In this case, the experimental averaged height of the

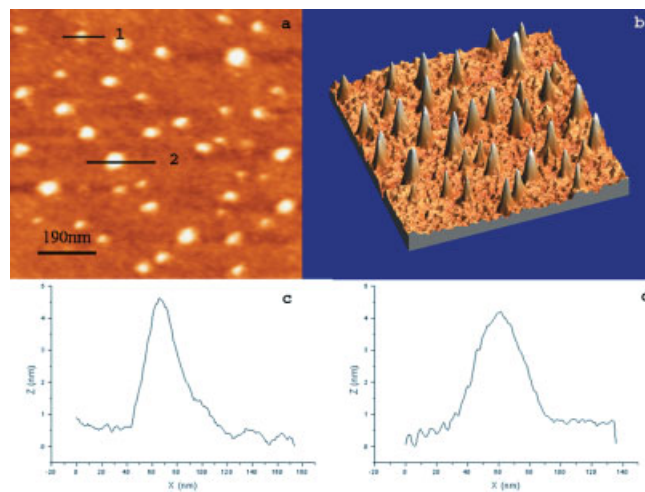


Fig. 2. AFM images of a thin nanocomposite film, made from a polycarbonate polymeric matrix and the  $Mn_{12}$  complex, which has been treated with pure  $CH_2Cl_2$ . a) Topographical top-view image. b) The corresponding 3D image of the same area. c) Height profile at location marked 1 in (a). d) Height profile at location marked 2 in (a).

dots observed by AFM topography turned out to oscillate between 4 and 5 nm, which is in excellent agreement with the molecular end-to-end distance of 4 nm determined for the  $Mn_{12}$  complex. Moreover, the size of the dots appears to have become substantially more monodisperse, as expected for single molecules.<sup>[18]</sup> This provides further evidence that indeed truly individual  $Mn_{12}$  molecules are imaged here.

Magnetic force microscopy (MFM) was applied to study both the molecular image and the magnetic response of nanocomposite thin films. MFM uses a tip that is magnetized by covering it with magnetic material. This unfortunately leads to images of poorer quality than those previously obtained due to the thickening of the tip. However, it offers the possibility of mapping the magnetic behavior of objects on the studied film surface. In a first sweep, the AFM tapping mode is used whereas in the second sweep, which is carried out over the same area but with the tip retracted to be out of the topographical signal, the local magnetization of the sample is monitored. The top-view topographical image and the corresponding MFM images of thin films treated either with  $CH_2Cl_2$  and  $CH_2Cl_2$ /hexane vapor are shown in Figure 3. MFM images clearly indicate a magnetic gradient response exactly corresponding to the molecular position found by topographic im-

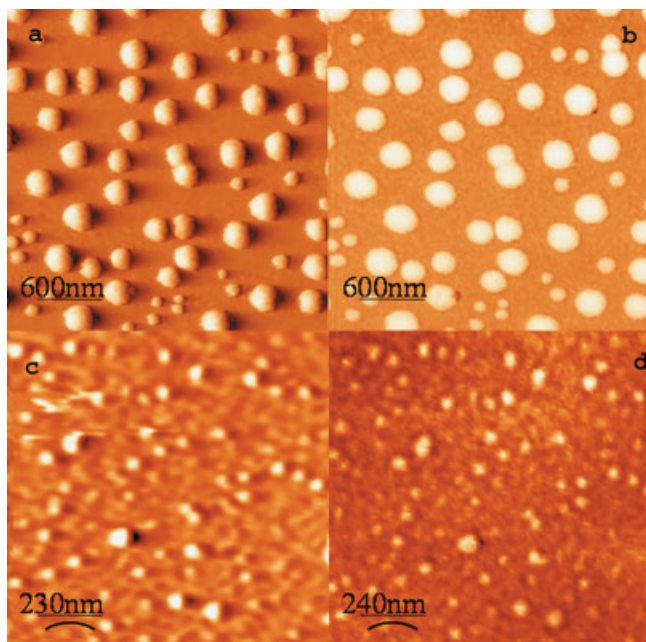


Fig. 3. MFM images of nanocomposite thin films treated with  $\text{CH}_2\text{Cl}_2$ /hexane (1:1) (a,b) and with  $\text{CH}_2\text{Cl}_2$  (c,d). a,c) Topographical images taken with the magnetic tip. b,d) Magnetic images of the same area after retracting the tip by 30 nm.

aging. This fact is the best confirmation to unequivocally assign the dots observed by high-resolution AFM images to single  $\text{Mn}_{12}$  molecules or aggregates of such molecules rather than to any impurity or small polymeric crystallites.

Magnetic characterization of the nanocomposite thin films was initially performed by means of ac magnetic susceptibility measurements at different frequencies using several wrinkled thin films compressed into the sample holder. Consequently, this sample contains a collection of randomly oriented and fixed  $\text{Mn}_{12}$  molecules inside the polymeric matrix. As shown in Figure 4a, the thin films show two out-of-phase ac frequency-dependent peaks, with an effective potential barrier ( $U_{\text{eff}}$ ) of 36 K and magnetic relaxation time  $\tau_0 = 10^{-9}$  s for the low-temperature peak, and 56 K and  $\tau_0 = 4 \times 10^{-8}$  s for the high-temperature peak, respectively. At this point, it is important to mention that both frequency-dependent peaks exhibit the same relative intensity and values for  $\tau_0$  and  $U_{\text{eff}}$  as those observed for a polycrystalline sample of the  $\text{Mn}_{12}$  complex. To get more insight into the orientation of the molecular complexes inside the bulk polymeric matrix, several thin films were aligned and stacked together. Magnetic measurements were then performed with the magnetic field applied parallel and perpendicular to the surfaces of the stacked films. The field-dependence of magnetization shown in Figure 4b indicates that most of the molecules of the  $\text{Mn}_{12}$  complex of the thin film tend to align their easy-magnetization axis in some direction inside the plane. This fact also explains why hysteresis is only observed when the field is applied parallel to the surface, and is not detected otherwise. Such alignment may be explained by considering the internal structural reorganization of the polymeric matrix during the swelling process. In-

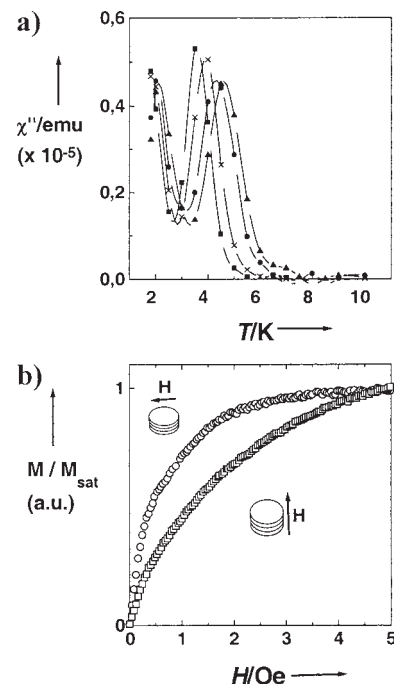


Fig. 4. a) Out-of-phase component of magnetic susceptibility for the nanocomposite thin films at four different frequencies ( $\blacksquare$  3 Hz,  $\times$  10 Hz,  $\circ$  50 Hz,  $\blacktriangle$  100 Hz). b) Field dependence of magnetization for several stacked films placed parallel ( $\circ$ ) and perpendicular ( $\square$ ) to the direction of the applied magnetic field. For the parallel case saturation is achieved at 2.5 T, whereas for the perpendicular case the saturation occurs at fields larger than 5 T.

deed, when the solvent molecules penetrate the film and cause it to swell, the glass-transition temperature is reduced to ambient temperature. As a consequence, restrictions on the rotation of the polymer chains are removed, and this therefore permits the movement of molecules that are inside the matrix. After drying the solvent, an energetically favorable polymeric conformation is readily adopted, resulting in the development of oriented microcrystalline domains under ambient laboratory conditions. In view of that,  $\text{Mn}_{12}$  molecules also tend to align during the swelling process forced by the microcrystalline polymeric environment and they remain oriented after drying the solvent. Further work to fully address this explanation is currently underway.

In summary, here we report a new, simple, and reliable methodology to address individual single-molecule magnets onto a thin film surface, which can be used as magnetic quantum bits for information storage or quantum computing.<sup>[19]</sup> The advantages of this approach are considerable. Firstly, the polymeric matrix plays a critical role in stabilizing the SMM as well as in enhancing the overall mechanical strength of the film.<sup>[20]</sup> The lack of stability of LB films or the use of rather aggressive techniques such as chemical or physical vapor deposition can thus be circumvented. Secondly, polycarbonates are commercially important and technologically interesting polymers that have a combination of properties not found in any other plastic, including very high impact strength, creep resistance, optical clarity, and a low moisture absorption. And finally, the resulting nanocomposite thin films are fully com-

patible with today's magnetic and magneto-optical storage technologies, where polycarbonate resins are used as the basic support for the fabrication of disks. Therefore, the nanocomposite thin films reported here can be easily transferred or even directly prepared by a spin-coating method onto a disk support without losing continuous nanoscopic characteristics.

### Experimental

The Mn<sub>12</sub> complex used to prepare the nanocomposite was [Mn<sub>12</sub>O<sub>12</sub>(O<sub>2</sub>-CC<sub>6</sub>H<sub>4</sub>C<sub>6</sub>H<sub>5</sub>)<sub>16</sub>(H<sub>2</sub>O)<sub>4</sub>], which has recently been described [21]. Polycarbonate films with 4 wt.-% of molecularly dispersed complex were cast onto a glass surface. Spectrochemical characterization of the resulting films with a typical thickness of 10–15 μm, showed no evidence of any decomposition process and therefore gave good indications that the Mn<sub>12</sub> complexes embedded in the polymeric matrix were stable. Next, the films were treated with solvent vapor of CH<sub>2</sub>Cl<sub>2</sub> or 1:1 CH<sub>2</sub>Cl<sub>2</sub>/hexane mixtures by simply placing the film at the top of a flask containing a small amount of the organic solvent for 5 min. The films were then dried, resulting in a glassy material with no detectable porosity. AFM/MFM measurements were performed with a commercial scanning force microscope from Nanotec. The AFM images, were taken in tapping mode, with Olympus silicon cantilevers with a spring constant of 0.75 N m<sup>-1</sup> and a resonance frequency of 80 kHz. The MFM images were taken with Nanosensors silicon cantilevers (spring constant 4 N m<sup>-1</sup>, 72 kHz resonance frequency) which were covered with 50 nm of cobalt. The scan lift-height for the magnetic images was 30 nm. With the magnetic cantilever, the first scan reveals the topography and after retracting a certain height; the second scan reveals the magnetic mapping of the same area. AC and DC magnetic measurements were collected with a Quantum Design MPMS2 SQUID magnetometer equipped with a 5 T magnet with operating frequencies from 3 to 1500 Hz, and temperatures from 1.8 K to 400 K.

Received: September 30, 2002

- [1] R. Sessoli, D. Gatteschi, A. Caneschi, M. A. Novak, *Nature* **1993**, 365, 141.
- [2] J. R. Friedman, M. P. Sarachick, J. Tejada, R. Ziolo, *Phys. Rev. Lett.* **1996**, 76, 3830.
- [3] J. M. Hernandez, X. X. Zhang, F. Luis, J. Bartolomé, J. Tejada, R. Ziolo, *Europhys. Lett.* **1996**, 35, 301.
- [4] L. Thomas, F. Lioni, R. Ballou, D. Gatteschi, R. Sessoli, B. Barbara, *Nature* **1996**, 383, 145.
- [5] J. A. A. J. Perenboom, J. S. Brooks, S. Hill, T. Hathaway, N. S. Dalal, *Phys. Rev. B* **1998**, 58, 330.
- [6] L. Bokacheva, A. D. Kent, M. A. Walters, *Phys. Rev. Lett.* **2000**, 85, 4803.
- [7] A. D. Kent, Y. Zhong, L. Bokacheva, D. Ruiz, D. N. Hendrickson, M. P. Sarachick, *Europhys. Lett.* **2000**, 49, 521.
- [8] W. Wernsdorfer, R. Sessoli, *Science* **1999**, 284, 133.
- [9] D. Ruiz, Z. Sun, B. Albelá, K. Folting, J. Ribas, G. Christou, D. N. Hendrickson, *Angew. Chem. Int. Ed.* **1998**, 37, 300.
- [10] H. J. Eppley, H.-L. Tsai, N. De Vries, K. Folting, G. Christou, D. N. Hendrickson *J. Am. Chem. Soc.* **1995**, 117, 301.
- [11] L. Krusin-Elbaum, T. Shibauchi, B. Argyle, L. Gignac, D. Weller, *Nature* **2001**, 410, 444.
- [12] E. M. Chudnovsky, J. Tejada, *Macroscopic Quantum Tunneling of the Magnetic Moment*, Cambridge University Press, Cambridge **1998**.
- [13] E. Del Barco, N. Vernier, J. M. Hernandez, J. Tejada, E. M. Chudnovsky, E. Molins, G. Bellesa, *Europhys. Lett.* **1999**, 47, 722.
- [14] M. Clemente-León, H. Soyer, E. Coronado, C. Mingotaud, C. J. Gómez-García, P. Delhaès, *Angew. Chem. Int. Ed.* **1998**, 37, 2842.
- [15] A. A. D'Archivio, L. Galantini, A. Biffis, K. Jerábek, B. Corain, *Chem. Eur. J.* **2000**, 6, 794.
- [16] Molecular Modeling System. HyperChem 5.02 for Windows 95/NT, Autodesk, Inc.
- [17] K. Takada, D. J. Díaz, H. D. Abruña, I. Cuadrado, B. González, C. M. Casado, B. Alonso, M. Morán, J. Losada, *Chem. Eur. J.* **2001**, 7, 1109.
- [18] The heights of a few single molecules are smaller than the average 4–5 nm. Such a result can be ascribed to molecules that have not completely emerged to the surface of the films.
- [19] J. Tejada, E. M. Chudnovsky, E. del Barco, J. M. Hernandez, T. Spiller, *Nanotechnology* **2001**, 12, 181.

- [20] C. Castro, J. Ramos, A. Millán, J. González-Calbet, F. Palacio, *Chem. Mater.* **2000**, 12, 3681.
- [21] D. Ruiz-Molina, P. Gerbier, E. Rumberger, D. B. Amabilino, I. A. Guzei, K. Folting, J. C. Huffman, A. Rheingold, G. Christou, J. Veciana, D. N. Hendrickson, *J. Mater. Chem.* **2002**, 12, 1152.

## Electrophosphorescence from a Conjugated Copolymer Doped with an Iridium Complex: High Brightness and Improved Operational Stability\*\*

By Xiong Gong, Jacek C. Ostrowski, Guillermo C. Bazan,\* Daniel Moses,\* Alan J. Heeger, Michelle S. Liu, and Alex K.-Y. Jen

By utilizing triplet-based emitting centers in polymer and organic light-emitting diodes (PLEDs and OLEDs), and thereby capturing both singlet and triplet excited states, the internal quantum efficiency can, in principle, be increased to 100%.<sup>[1,2]</sup> The utilization of triplet emitters to improve efficiencies was proposed by several groups.<sup>[3–8]</sup> Recently, considerable progress has been demonstrated with electrophosphorescent OLEDs (based on small molecules) and PLEDs (based on polymers) as the host materials, and heavy-metal (Pt, Ir, Os) complexes and rare-earth metal complexes as the guest.<sup>[3–13]</sup>

With the addition of the phosphorescent guest, emission takes place either by Förster energy transfer from the host to the singlet excited state of the guest complex followed by intersystem crossing to the guest triplet state, or directly by electron and hole trapping on the metal–organic complex. Dexter energy transfer can also enable direct transfer from the triplet of the host to that of the guest.

For the iridium heavy-metal complexes, the emission originates from the triplet excited state to the ground state. By using different ligands, this triplet phosphorescence can be

[\*] Prof. G. C. Bazan, Dr. D. Moses, Dr. X. Gong, J. C. Ostrowski, Prof. A. J. Heeger  
Institute for Polymers and Organic Solids  
University of California at Santa Barbara  
Santa Barbara, CA 93106-5096 (USA)  
E-mail: bazan@chem.ucsb.edu; mooses@ipos.ucsb.edu

Prof. G. C. Bazan  
Department of Chemistry, University of California at Santa Barbara  
Santa Barbara, CA 93106 (USA)

Prof. A. J. Heeger  
Department of Physics and Materials Department  
University of California at Santa Barbara  
Santa Barbara, CA 93106 (USA)

M. S. Liu, Prof. A. K.-Y. Jen  
Department of Materials Science and Engineering  
University of Washington, Roberts Hall  
Box 352120, Seattle, WA 98195-2120 (USA)

[\*\*] This work was supported by the Mitsubishi Chemical Center for Advanced Materials at UCSB and the Air Force Office of Scientific Research through the MURI Center ("Polymeric Smart Skins"), Charles Lee, Program Officer. X. Gong is grateful to Dr. Gang Yu and Dr. Runguang Sun of Dupont Displays Corporation for valuable discussion. J. C. Ostrowski is a Kodak fellow and G. C. Bazan thanks the NSF for financial support (NSF CHE 0098 240). A. K.-Y. Jen and M. Liu thank the Air Force Office of Scientific Research for support through the MURI Center ("Polymeric Smart Skins"). M. Liu thanks the Nanotechnology Center at the University of Washington and PNNL for the Joint Institute Nanotechnology Fellowship.